Journal of Applied Fluid Mechanics, Vol. 13, No. 6, pp. 1727-1741, 2020.
Available online at www.jafmonline.net, ISSN 1735-3572, EISSN 1735-3645.
DOI: 10.47176/jafm.13.06.31454

Numerical Simulation of Ventilated Cavitation Evolution with an Insight on How Ventilation Influences Pressure Fluctuation and Cavitation Noise

A. Yu[1†], Z. H. Qian[1], J. J. Ji[2], Q. H. Tang[3], H. X. Chen[4] and D. Q. Zhou[1]

[1] *College of Energy and Electrical Engineering, Hohai University, Nanjing, 210098, China*
[2] *Beijing Institute of Space Launch Technology, Beijing 100190, China*
[3] *College of Water Conservancy and Hydropower Engineering, Hohai University, Nanjing, 210098, China*
[4] *College of Agricultural Engineering, Hohai University, Nanjing, 210098, China*

†*Corresponding Author Email: yu_an@hhu.edu.cn*

(Received February 8, 2020; accepted April 13, 2020)

ABSTRACT

Cavitation occurred in hydraulic machines can generate severe pressure fluctuations and induce high-pitched noise. Ventilated cavitation (inject air into the cavitating flow) is one of the most effective ways to control cavitation and then alleviate the noise and fluctuations. Thus, the evolution of ventilation cavitation around a NACA0015 hydrofoil was numerically investigated with a modified model. The results indicated that the ventilated cavitation consists of two parts: the attached cavity which attached to the leading edge of the hydrofoil and the detached cavity which detached from the hydrofoil surface. With the air injection increased, the detached cavity becomes larger. Besides, the ventilated cavity evolves periodically along with two opposite vortexes which fall off in turn near the tailing edge of the hydrofoil. Among three ventilation volumes, an air injection of 250 L/min presents the best alleviation on pressure fluctuation induced by cloud cavitation. The acoustic analysis indicated that air injection is an effective way to alleviate the cavitation induced noise. With air injected into the flow, two new types noises induced by the ventilated cavitation has been detected by monitoring points along the upper side and behind of the hydrofoil: the lower frequency noise induced by the waving of attached cavity and the higher frequency noise induced by the shedding of the detached cavity. While with the air injection increased, both of the two types noises increased. The acoustic and dynamic patterns under different air injection conditions are able to provide guidance in engineering application.

Keywords: Ventilated cavitation; NACA0015 Hydrofoil; Pressure fluctuation; Cavitation noise.

NOMENCLATURE

C	chord length		
C_μ	0.09	u	velocity
C_3	1.0	V_{cav}	cavitation volume flow rate
Fe	evaporation coefficient		
Fc	condensation coefficient	λ	filter scale
p’	sound pressure	μ_m	mixture molecular viscosity
p	pressure	μ_t	turbulent viscosity
P_v	vaporization pressure	ρ_m,	fluid density
Q_{out}	volume flow at the outlet	σ	cavitation number
Q_{in}	volume flow at the inlet	σ_s	surface tension coefficient
R	bubble diameter	κ	surface curvature
$r$nuc	nucleation bubble diameter	$\delta(f)$	dirac-δ function
T_{ij}	lighthill stress tensor	ϕ	level Set function

1. INTRODUCTION

Cavitation is a common phenomenon that has a phase transition between water vapor and liquid water. It mainly occurs in the areas where the pressure drops below the saturated steam pressure. Cavitation is a complicated problem and it occurs widely in hydraulic machines, causing cavitation erosion, high-pitched noise, and pressure fluctuations. Therefore, it's essential to investigate and understand the cavitation mechanism fully because of its widespread and undesirable features.

Experiment around hydrofoil was always the main method of studying the cavitation mechanism. Previous experiments show that cavitation shows different characteristics with cavitation number decreased, such as cavitation inception with single bubbles, sheet cavity, cloud cavity and supercavitation (Wang *et al.* 2001). Kravtsova *et al.* (2014) proved that the PIV method is usable for the measurement of instantaneous velocity in the vapor phase. They also found that the leading edges affect the cavitation inception strongly through an experiment. Kawanami *et al.* (1997) investigated the generation mechanism of cloud cavitation around hydrofoils in a water tunnel.

With the development of computer technology, computational fluid dynamics (CFD) is widely used in the cavitating investigation. The investigations of cavitation evolution became a deeper based CFD method. Bal *et al*. (2001) obtained the integral equation deduced by Green's theorem. Based on this equation, cavitating hydrofoil moving with constant speed could be modeled. Ji *et al*. (2010) employed the modified RNG k-ε turbulence model and compute the cavitating flow around a hydrofoil. Long *et al*. (2017) used the integral method and modified turbulence model, receiving numerical results validated with experimental data.

In hydraulic turbines, cavitation is an adverse phenomenon, causing vibrations, noise and electric network fluctuation (Li *et al*. 2016, Luo *et al*. 2016 and Pendar and Roohi 2016). As a research challenge to avoid cavitation, many investigations have been done to explore its mechanism.

Pressure fluctuations induced by cavitating flow have been studied for a long time and the mechanism of pressure fluctuations has been investigated thoroughly. Li *et al*. (2015) analyzed the relationship between flow structure and pressure fluctuations, he also provided a reference for furthering mechanism investigation about hydrofoil vibration induced by cavitation. Zhang *et al*. (2015) focused on NACA66's numerical simulation and obtained the features of pressure fluctuation induced by the cavitation evolution. Gao *et al*. (2015) analyzed cavitation characteristics and vibration response around NACA66 experimentally. The vorticity transport equation was introduced by Liu *et al*. (2019) to reveal the interaction of cavitation and vortex. Ji *et al*. (2014) found the cavity volumetric acceleration is proportional to the pressure fluctuations. The study also reveals the rules of pressure propagation and pressure distribution around the hydrofoil.

Compared with pressure fluctuation investigation, flow-induced noise has not been studied thoroughly and the numerical simulation method of noise still needs to be improved. Kim *et al*. (2016) focused on the cavitating flow noise problems around the hydrofoil and the hydro-acoustic noise was predicted. They also inquired into the effects of viscous flux vectors (Kim *et al*. 2018) and turbulence models (Kim *et al*. 2017). Seo *et al*. (2018) presented a direct numerical prediction procedure for the noise radiated by the cavitating flow. Ku *et al*. (2017a) applied the acoustic analogy to predict flow-induced noise and analyzed the source of the noise. Based on the previous study, they reduced the error of numerical calculation in virtue of quadrupole-corrected FW-H equation (Ku *et al*. 2017b).

The experimental study of cavitation erosion is the most common and accurate method. Experimental study takes a long time, so much researches have been done to study by numerical method. Kato *et al*. (1996) proposed a quantitative prediction scenario of cavitation erosion without a model test. Dular *et al*. (2006) developed a cavitation erosion model by combining cavitation erosion and visual effects. The predicted damage of this model related well to the experimental results. Blume and Skoda (2019) employed the statistical evaluation of collapsing voids, obtaining wall load collectives in good agreement with experimental data. Cheng *et al*. (2018) investigated cavitation erosion in a water jet experimentally and the theoretical model can verify cavitation erosion pits phenomenon as well as experimental results.

As an effective way proposed to alleviate those serious problems mentioned upfront, ventilation has been widely applied to engineering practices. To better understand this method thoroughly, a wide range of experimental and computational researches that deal with those problems have been made. Among these studies, hydrofoil, as a typical model of underwater vehicles, has been focused. For instance, experimental methods have been improved by Lee *et al*. (2013) to develop the necessary algorithms to analyze irregularly shaped bubbles and the bubble size and velocity distribution. Liu *et al*. (2018) used experimentl methods to investigate the ventilated partial cavitating flow structure at different angles of attack and it was found that the angle of attack has a significant effect on ventilated cavitating flow structures. Qin *et al*. (2019) conducted the experimental investigation on the cavity regime and the corresponding geometric characteristic of ventilated partial cavitation. The distribution of these cavity regimes over Froude number and ventilation coefficient is summarized in a regime map and the geometric characteristic of ventilated partial cavitation characterized by the cavity length was examined. What's more, calculation methods are widely used in many studies. Research about the low-drag cavitating hydrofoil indicates that ventilation can improve the hydrofoil performance (Kopriva and Arndt 2008). Jianhong Guo *et al.*

(2010) calculated and observed different gas leakage regimes at the aft of ventilated cavities and general characteristics of the gas leakage regimes and cavity morphology were predicted. Zhou *et al.* (2019) simulated the ventilated the interaction between the natural cavitation and ventilated cavitation around a baase-ventilated hydrofoil based on OpenFOAM. According to the results, the natural cavitation on the hydrofoil surface tends to be depressed by the ventilation cavitation at the base of the hydrofoil. Karn *et al.* (2014) investigate the three-dimensional ventilated super cavities on the disk and blunted cavitators (i.e. ventilated hydrofoil) and peculiarities caused by gravity effect presence of the cavitator angle of attack are discussed. Chen and Lu (2005) studied the unsteady process of ventilated cavities around a 2D hydrofoil. The results suggest that the ventilation rate is an important parameter in determining the morphology of the cavity. With more air through an orifice in the 2D hydrofoil, it can be identified that a high ventilation rate can induce a two-phase interface fluctuation and make the ventilated cavitating flow show a periodically characteristic. Additionally, there is research employed both numerical and experimental methods. Yu *et al.* (2019) proposed research analyzing the bubble evolution around a NACA0015 hydrofoil. The simulation, which is confirmed by experimental results, reveals that the ventilation injected from the leading edge of the hydrofoil accelerates the vapor cavity's growth and leads to an increase in cavity shedding frequency. Besides, it is also observed that the pressure fluctuation is suppressed to a great extent with a suitable air flow rate.

Ventilation is one of the most effective ways to control cavitation and then alleviate the fluctuations and noise. However, research about the effects of ventilation on pressure fluctuation and flow induced noise has not been fully investigated, and the impact of different ventilation volume on its alleviation effect is still not clear. Thus, the present study investigated the pressure fluctuation and flow induced noise around a NACA0015 hydrofoil, using a modified simulation method. Moreover, a NACA0015 ventilation model was introduced to explore the effects of ventilation on pressure fluctuation and cavitation noise. It is noteworthy that two typical cavitation numbers and three ventilation volumes were selected to investigate the features and patterns of air injections in different conditions; therefore, the acoustic and dynamic pattern under different conditions can provide instruction and guidance in engineering practices.

2. MATHEMATICAL MODEL

2.1 Basic Equations

The homogeneous assumption was usually adopted in two-phase cavitating flow simulation, where the whole cavitation flow field can be considered as a flow field of a single homogeneous fluid and the density and dynamic viscosity of the flow field are time-varying.

Since surface tension is the main force act between the liquid and gaseous phase, the source term of the surface term was taken into consideration in the momentum equation.

The weighted average value of the corresponding parameters of two-phase is taken for the parameters of homogeneous fluid, and the basic equations the flow are listed as follows:

$$\frac{\partial \rho_m}{\partial t}+\frac{\partial(\rho_m u_j)}{\partial x_j}=0 \tag{1}$$

$$\rho_{\mathrm{m}}\left(\frac{\partial \boldsymbol{u}}{\partial t}+\boldsymbol{u}\cdot\nabla\boldsymbol{u}\right)=-\nabla p+\nabla\cdot\left[\mu(\nabla\boldsymbol{u}+(\nabla\boldsymbol{u})_{\mathrm{c}})\right]+\sigma_{\mathrm{s}}\kappa\delta(d)\boldsymbol{n} \tag{2}$$

The last term is the surface tension term. In order to convert the surface tension force into a calculable term, Level set function is adopted.

2.2 Turbulence Model

The *k*-*ε* model is preferred due to its less computing resources requirement and satisfactory simulation stability. Nevertheless, the viscosity coefficient is calculated by a function of turbulent kinetic energy and turbulent dissipation rate in the *k*-*ε* model, which means the *k*-*ε* model forecasts the viscous coefficient excessively and underestimates the instability of cavitation flow. To amend the defect of the standard *k*-*ε* model in catching cavitation flow, a Filter-based Model (FBM) is adopted which set different turbulent viscosity μ according to different turbulent scales:

$$\mu_{T_{FBM}}=\frac{C_\mu \rho_m k^2}{\varepsilon}F_{FBM} \tag{3}$$

$$F_{FBM}=\min\left(1,C_3\frac{\lambda.\varepsilon}{k^{\frac{3}{2}}}\right) \tag{4}$$

2.3 Cavitation Model

Zwart Cavitation Model is selected in the investigation. The mass transfer equation for water vapor is defined as follows:

$$\frac{\partial(\rho_v\alpha_v)}{\partial t}+\frac{\partial(\rho_v\alpha_v u_i)}{\partial x_i}=\dot{m}^+ +\dot{m}^- \tag{5}$$

where ρ_{v} is the vapor density, and α_{v} represents the vapor volume fraction. The interaction between different cavitation bubbles is ignored and the nucleation density decreases with the increase of vapor volume fraction. To take the influence of non-condensable air into cavitation evolution, the evaporation and condensation source terms in Zwart Model are modified as follows:

$$\dot{m}^+ = C_{\mathrm{e}}\frac{3\rho_{\mathrm{v}}\max(\alpha_{\mathrm{nuc}},\alpha_{\mathrm{a}})(1-\alpha_{\mathrm{v}})}{R_{\mathrm{b}}}\sqrt{\frac{2}{3}\frac{\max(p_{\mathrm{v}}-p,0)}{\rho_{\mathrm{l}}}} \tag{6}$$

$$\dot{m}^- = C_{\mathrm{c}}\frac{3\rho_{\mathrm{v}}\alpha_{\mathrm{v}}}{R_{\mathrm{b}}}\sqrt{\frac{2}{3}\frac{\max(p-p_{\mathrm{v}},0)}{\rho_{\mathrm{l}}}} \tag{7}$$

where F_e is the evaporation coefficient, r_{nuc} the nucleation site volume fraction, R the bubble diameter, P_v the vaporization pressure, F_c the condensation coefficient. The coefficients above are set as follows: $r_{nuc}=5.0\times10^{-4}$m, $R=1.0\times10^{-6}$m, $F_e=50$, $F_c=0.01$.

2.4. FW-H Equation

The FW-H Equation is employed to predict the hydro-acoustic waves radiating from the cavitation flow. The form of the FW-H Equation is derived from the continuity equation and the N-S equation, describing the quadrupole, dipole and monopole acoustic source terms detailly based on the acoustic analogy. The FW-H equation is as follows:

$$\frac{\partial^2 p}{\partial t^2}-c^2\frac{\partial^2 p}{\partial x_i^2}=\frac{\partial^2 T_{ij}}{\partial x_i \partial x_j}-\frac{\partial}{\partial x_i}\left[P_{ij}\delta(f)\frac{\partial f}{\partial x_j}\right]+\frac{\partial}{\partial t}\left[\rho_0 u_i(f)\frac{\partial f}{\partial x_j}\right] \tag{8}$$

where p' is the acoustic pressure, $\delta(f)$ the Dirac-δ function, T_{ij} the Lighthill tensor.

$$T_{ij}=\rho u_i u_j+P_{ij}-c^2\rho\delta_{ij} \tag{9}$$

$$P_{ij}=p\delta_{ij}-\mu\left(\frac{\partial u_i}{\partial x_j}+\frac{\partial u_j}{\partial x_i}-\frac{2}{3}\frac{\partial u_k}{\partial x_k}\delta_{ij}\right) \tag{10}$$

The first term of the right side of the equation is quadrupole acoustic source, which represents high-frequency noise related to turbulent velocity fluctuations. The second term is the dipole acoustic source which considers a stationary solid body in the flow field as a low-frequency noise source. The third term is the monopole acoustic. It causes acoustic pressure which links with the rate of cavitation volume changes referring to cavitation bubble development and collapse in this article. It's noteworthy that the quadrupole terms' acoustic energy is up to the 8th power of the Mach number. Hence, the quadrupole acoustic source is far less than the other two acoustic sources in this article and can be ignored.

3. COMPUTATIONAL DOMAIN AND SIMULATION CONDITIONS

The experiments on natural cavitation and ventilation cavitation were conducted in the high-speed water tunnel testbed of BIT (Beijing Institute of Technology). Therefore, the computational domain was designed in reference to the testbed. Considering the two-dimensional characteristics of the NACA0015 hydrofoil and the economization of computational resources, a symmetry boundary condition was set for the side-walls of the computational tunnel. The computational domain configured for simulation is presented in Fig. 1. The hydrofoil attack angle was set at 6º. The chord length (C=0.07m) and domain height (h=0.19m) are identical with those configured in the experiments. The inlet boundary is 3C ahead of the hydrofoil, where the inflow velocity (i.e. Vx) was set at 7.2m/s. The pressure outlet was set 5.5C behind the hydrofoil. In the present investigation, a constant temperature of 298K was utilized, where the saturated vapor pressure p_v and the liquid water density are 3,540Pa and 998kg/m^3 respectively. Thus, the cavitation number σ (= (p_{out} - p_v)/(0.5$\rho_l u_\infty^2$)) is varying with the outlet pressure value. The locations of the monitor points are showing in Fig. 2. They are named as D1 to D10 and B1 to B10 in order.

Two typical cavitation numbers (σ=1.075 and σ=0.65) and three injected airflow rates (V_{air}=250L/min, 375L/min, 500L/min) were selected to investigate the characteristics of air injections in different conditions.

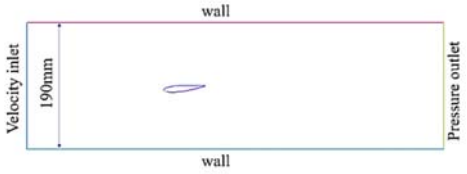

Fig.1. Computational domain and boundary conditions.

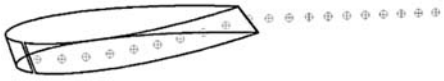

Fig.2. Locations of the monitor points.

4. RESULTS AND DISCUSSIONS

4.1 Ventilated Cavitation Evolution

4.1.1 Verification Test

Before the investigation, a verification test was conducted by comparing the numerical results to experimental data. The experiments were done in a high-speed water tunnel at Beijing Institute of Technology, while numerically simulation was conducted by using the ANSYS CFX. The experimental cavitation evolution with two typical cavitation numbers and three ventilated airflow rates are showing in Figs. 3., 4. and 5. The simulation results are shown with the vapor volume fractions. As shown in Fig. 3, the cavity attached to the leading edge is stable when no air is ventilated to the flow field at σ=1.075. When the air was injected, sheet cavitation is disrupted and nature cavitation changes to ventilation cavitation. The ventilated cavity consists of two parts: a steady attached cavity in the leading edge of the hydrofoil and an unsteady waving cavity detached from the hydrofoil surface. Figure 4 shows the cavitation evolution at σ=0.65 during a period of cloud cavitation. The cavitation evolution of three ventilation volumes is shown in Fig. 5 respectively. As the same as the condition of σ=1.075, cloud cavitation is suppressed and the bubbles detached from the leading edge become larger as the air injection increasing. Except for the difference in bubble size, the motion patterns of fluid in the flow field are similar in Fig. 3 and Fig. 4. Through the comparison of experiment and numerical

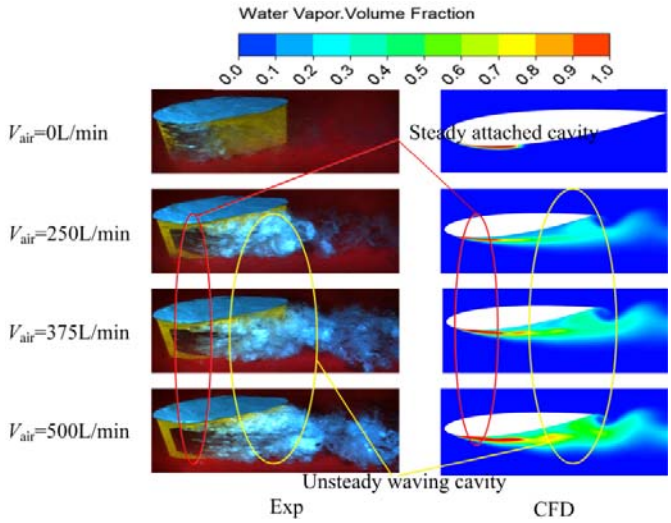

Fig. 3. Ventilated cavitation evolution at σ=1.075.

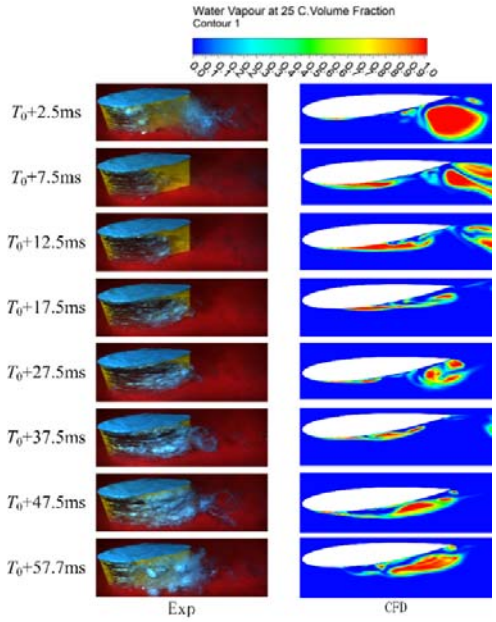

Fig. 4. Nature cavitation evolution at σ=0.65.

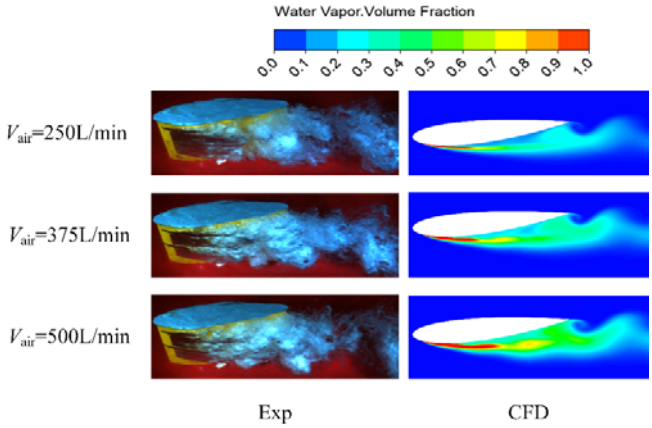

Fig. 5. Ventilated cavitation evolution at σ=0.65.

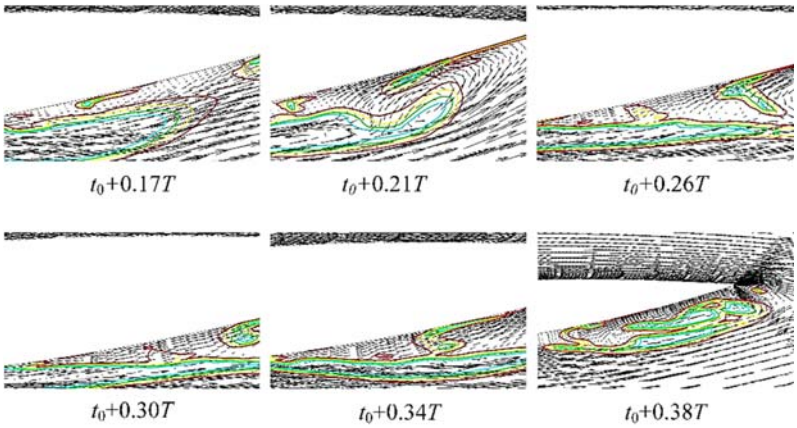

Fig. 6. Velocity vector field of Vair=0L/min (σ=0.65).

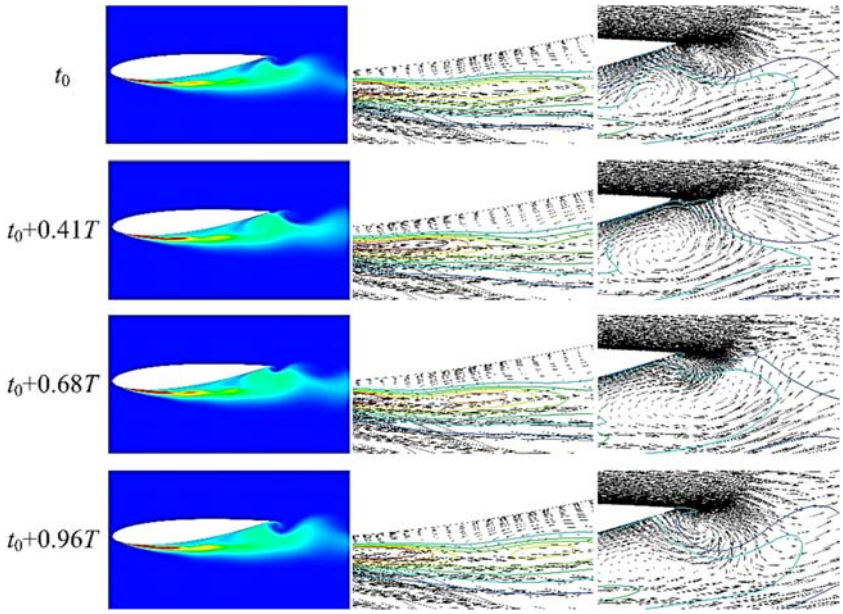

Fig. 7. Velocity vector field of Vair=375L/min (σ=0.65).

simulation, the simulation result is in good agreement with experimental data and simulation accuracy is therefore proven.

4.1.2 Cavitation Evolution

It can be seen from Fig. 3 to Fig. 5 that the cavitation evolution of different ventilation volumes shares the same characteristic. Therefore, two computational conditions (V_{air}=0L/min and V_{air}=375L/min at σ=0.65) were chosen to investigate the difference between nature cavitation and ventilated cavitation.

Figure 6 shows the velocity vector field of V_{air}=0L/min. When the attached cavity reaches its longest length (t_0+0.21T), a cavitation vortex will occur at the hydrofoil's tail. Then a re-entrant jet which points upstream is induced by the vortex (t_0+0.30T). When the re-entrant jet meets the mainstream, the attached cavity is cut off by the re-entrant jet and large-scale cloud cavity is detached from the hydrofoil surface with vortex motion (t_0+0.38T).

Figure 7 shows the velocity and volume fraction distributions of V_{air}=375L/min. As is shown in t_0 of Fig. 7, two vortices rotate in different directions near the hydrofoil's tail. The counterclockwise vortex induces the re-entrant jet. Different from nature cavitation, the re-entrant jet couldn't cut off the attached cavity because the injected air is consecutive and strong. Therefore, the attached cavity presents a wave shape. From t_0 to t_0+0.41T, the counterclockwise vortex grows and pushes the clockwise vortex away from the hydrofoil's tail. Meanwhile, the wake vortex detached from the tail is crest shaped. From t_0+0.41T to t_0+0.68T, the clockwise vortex reemerges from the tail and

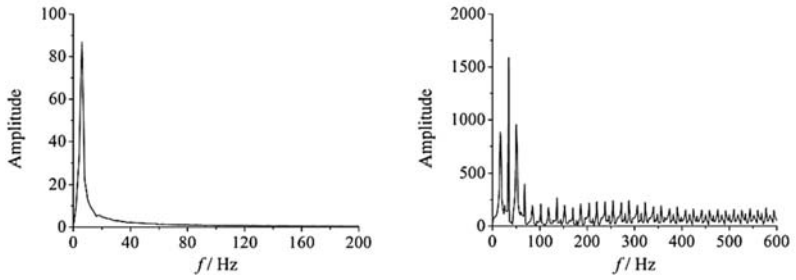

Fig. 8. Pressure fluctuation at D5 with two cavitation numbers.

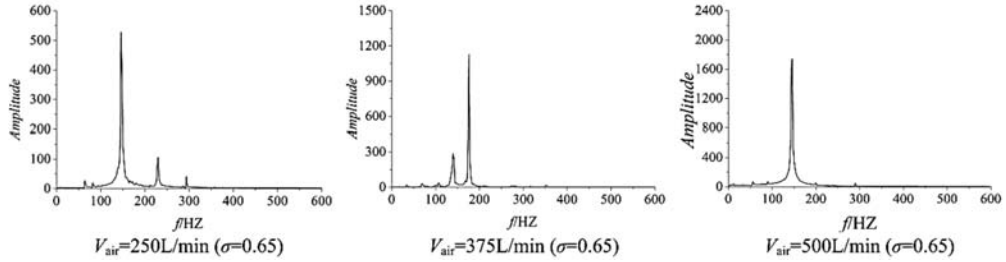

Fig. 9. Pressure fluctuations at D5 with air injection.

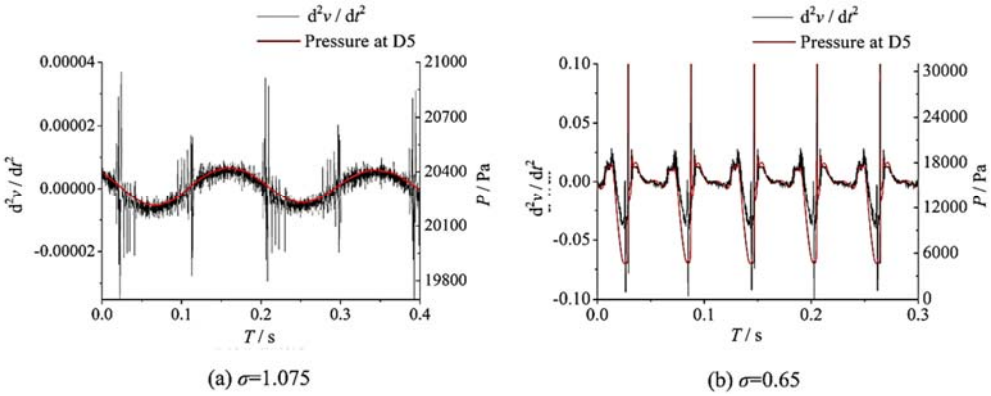

Fig. 10. Pressure fluctuations and cavity volumetric acceleration for nature cavitation.

grows, truncating the counterclockwise vortex. At this moment, the wake vortex detached from the tail has a trough shape. To $t_0+0.96T$, a new cycle begins.

4.2 Pressure Fluctuations

Cavitation is a completely unsteady phenomenon and can generate severe pressure fluctuations (Ji *et al*. 2018). As air injection is usually used to control nature cavitation, the characteristics of pressure fluctuations in the cavitating flow were investigated with and without air injection.

The pressure fluctuations at D5 with different cavitation numbers are showing in Fig. 8. The cavity attached to the leading edge of the hydrofoil and remained rather steady at σ=1.075. Thus, the pressure fluctuations induced by the natural sheet cavitation is not severe (the amplitude is only 86Pa) and can be ignored. While at σ=0.65, the natural cavitation becomes a fully developed cloud cavitation, as showing in Fig. 4. With the periodical developing and shedding off of the cavity, a series of pressure fluctuations were generated, as showing in Fig. 8 (b). The amplitude of the dominant pressure fluctuation is about 1600 Pa.

Air injection is an effective way to control the natural cavitation and alleviate the pressure fluctuations in cavitating flows. Pressure fluctuations at D5 with different injected airflow rates are showing in Fig. 9. The pressure with low frequency is completely suppressed by air injection. But with air injected into the flow, a high-frequency pressure fluctuation appeared and the amplitude increased with the injected air flow rate. With V_{air}=500L/min, the amplitude is higher than that of natural cavitation. But it is still an effective way to alleviate the pressure fluctuations induced by the

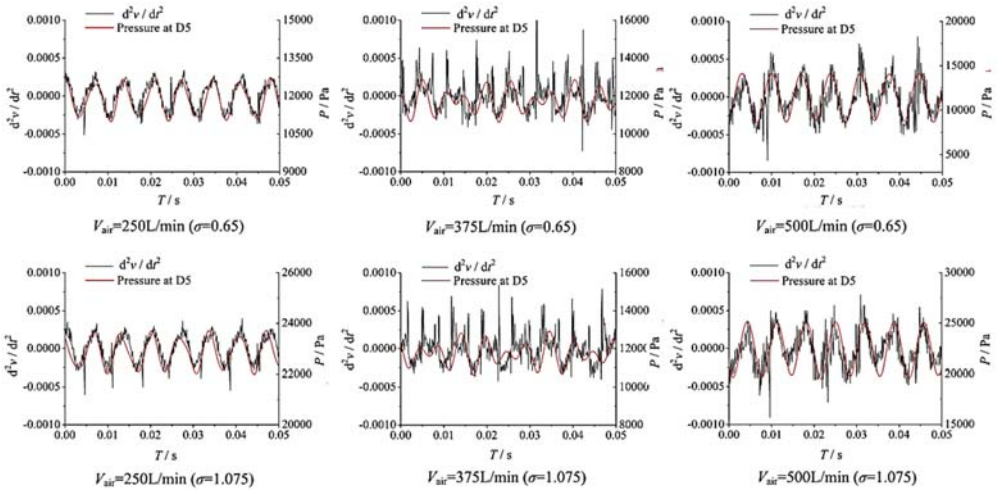

Fig. 11. Pressure fluctuations and cavity volumetric acceleration for ventilation cavitation.

natural cloud cavitation with suitable injected air flow rate, for example, V_{air}=250L/min in the present condition.

Based on the previous studies, the pressure fluctuations induced by cavitation is closely connected to the evolution of the cloud cavity and is proportional to the cavity volumetric acceleration (Ji *et al*. 2018), which is expressed by the formula as

$$P \propto \frac{d^2 v_{cav}}{dt^2} \tag{11}$$

To verify this conclusion, two nature cavitation conditions (σ=0.65 and σ=1.075) were analyzed. Pressure fluctuations and cavity volumetric acceleration are compared in Fig. 10. As shown in Fig. 10, the curve of cavity volumetric acceleration tracks the curve of pressure fluctuations remarkably well. What's more, it also shows the agreement between the theory and this investigation's numerical simulation.

When nature cavitation changes to ventilation cavitation, the gases in the flow field include water vapor and air. Therefore, the conclusion above should be modified. The conclusion is derived from the continuity equation, whose expression is as follows:

$$Q' = Q_{out} - Q_{in} = \frac{dv_{cav}}{dt} \tag{12}$$

With air injection increasing, both cavitation volume and air volume induce the variation in volume flow. Hence, the continuity equation of ventilation cavitation is as follows:

$$Q' = Q_{out} - Q_{in} = \frac{d(v_{cav} + v_{air})}{dt} = \frac{dv_{gas}}{dt} \tag{13}$$

The conclusion applicable to ventilation cavitation is as follows:

$$P \propto \frac{d^2 v_{gas}}{dt^2} \tag{14}$$

To verify the conclusion above, six conditions of ventilation cavitation (V_{air}=250L/min, 375L/min, 500L/min at σ=0.65 and 1.075) were analyzed. Figure 11 shows two curves respectively representing pressure fluctuations and gaseous phase volumetric acceleration. There is a good agreement between the curve of pressure fluctuations and the curve of gas volumetric acceleration. Deriving from the analysis upfront, the gaseous phase volumetric acceleration is proportional to the pressure fluctuations excited by ventilation cavitation.

With injected airflow rate increasing, the pressure fluctuation amplitude of V_{air}=250L/min (σ=0.65) is lower than those of V_{air}=0L/min, V_{air}=375L/min, V_{air}=500L/min (σ=0.65). Meanwhile, the pressure fluctuation amplitude of V_{air}=0L/min (σ=1.075) is lower than that of V_{air}=250L/min, V_{air}=375L/min, V_{air}=500L/min (σ=1.075). This phenomenon can be explained by the conclusion above that the pressure fluctuations excited by ventilated cavitation are proportional to the gaseous phase volumetric acceleration. Cloud cavitation (V_{air}=0L/min, σ=0.65) owns large-scale bubbles detached from hydrofoil, so it has a high cavity volumetric acceleration. With ventilation volume up to 250 L/min, cloud cavitation is disrupted and the cavity attaching to the leading edge becomes much more stable. But when ventilation volume gets larger, the morphology of the cavity shows more dramatic changes and the gaseous phase volumetric acceleration is higher. Therefore, the pressure of V_{air}=250L/min (σ=0.65) has the lowest fluctuation amplitude. While for sheet cavitation (V_{air}=0L/min, σ=1.075), the cavity has a stable shape and the cavity volumetric acceleration is relatively low. But ventilation cavitation (V_{air}=250L/min, 375L/min, 500L/min when σ=1.075) has a relatively high gaseous phase volumetric acceleration, and the

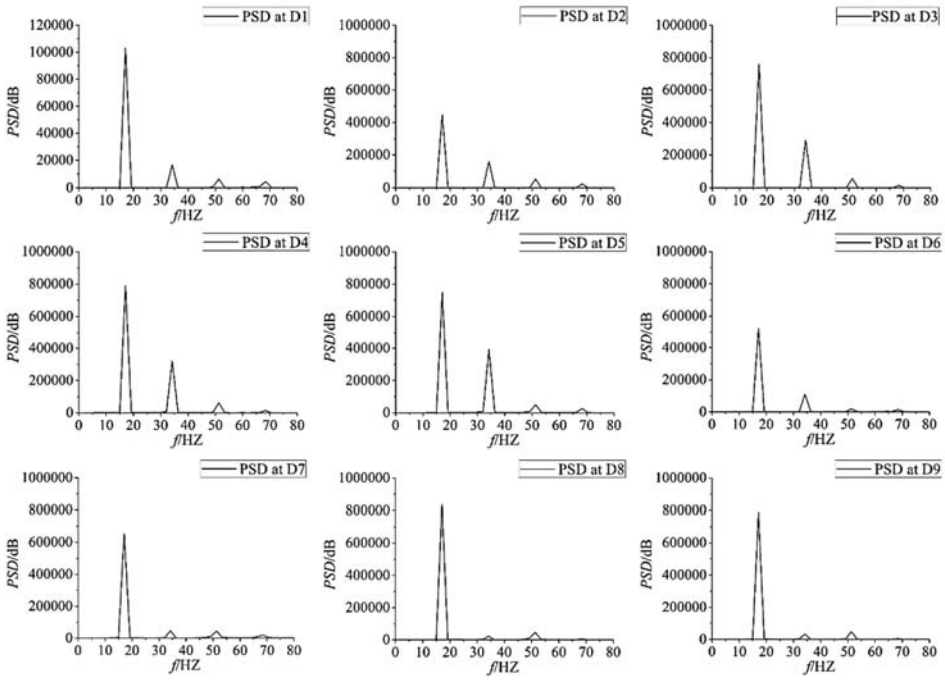

Fig. 12. Acoustic power spectral density of 9 points for σ=0.65.

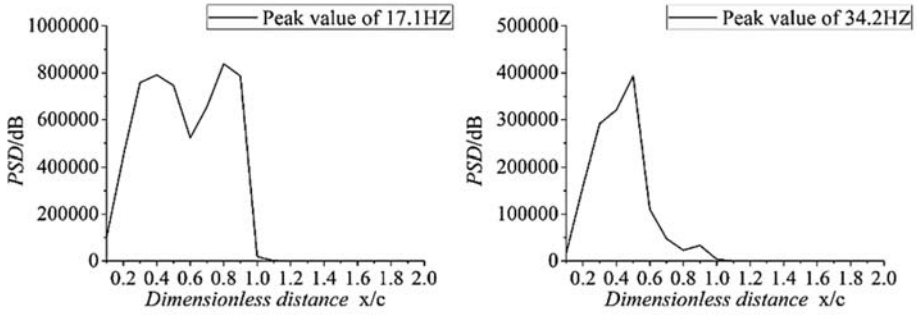

Fig. 13. Peak value of acoustic power spectral density of 20 points for σ=0.65.

pressure fluctuation amplitude of ventilated cavitation is, therefore, higher than sheet cavitation.

To summarize, air injection-induced new pressure fluctuations in the flow around the hydrofoil, but it is still an effective way to alleviate the pressure fluctuations induced by cloud cavitation (σ=0.65). While air injection is not capable to suppress the pressure fluctuation of sheet cavitation (σ=1.075).

4.3 Cavitation Flow-Induced Noise

4.3.1 Noise Pattern of Nature Cavitation

The previous investigations revealed the characteristics of natural cavitation induced noise around a NACA0015 hydrofoil (Yu *et al.* 2019). It is confirmed that with the decreasing of cavitation number, the magnitude of acoustic power spectral density (PSD) increased significantly, which can be attributed to their difference in cavitation evolution. Besides, the different sources of cavitation induced noise were identified. At the conditions of sheet cavitation, only one peak value of PSD is found which is due to the swelling and shrinking of the leading-edge cavity. At the conditions of cloud cavitation, however, two peak values of PSD are found as a result of superposition from leading-edge cavity and trailing vortex. Nevertheless, the influence of aeration on cavitation induced noise has not been further discussed. In this article, the noise pattern of both nature cavitation and ventilated cavitation is discussed and compared in detail.

For nature cavitation, water-vapor is the only gas-phase material included in the cavitating flow. Noise patterns of σ=0.65 and σ=1.075 are discussed in this part.

When σ=0.65, Acoustic power spectral density of 9 points below the hydrofoil presents evident features of cloud cavitation as shown in Fig. 12. For points D1 to D5, two peak values of PSD are observed.

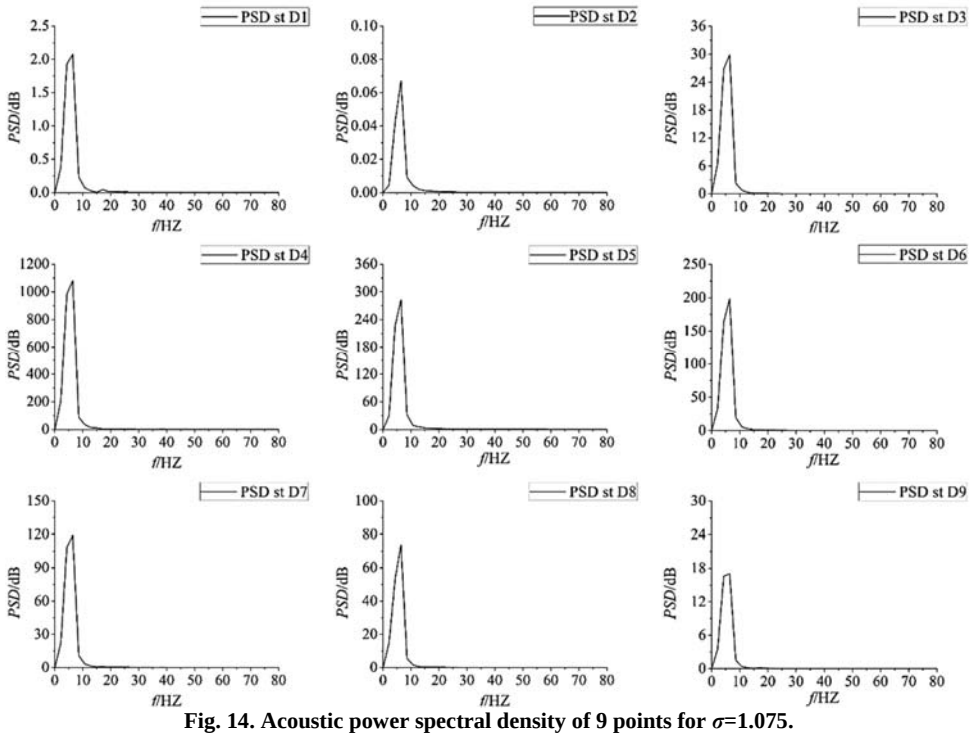

Fig. 14. Acoustic power spectral density of 9 points for σ=1.075.

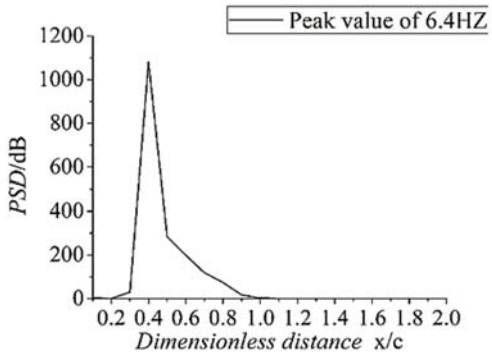

Fig. 15. Peak value of acoustic power spectral density of 20 points for σ=1.075.

For points D6 to D9, however, only one peal value is shown in the figure. This can be rightly explained by dividing the noise sources into two parts. The first peak value of 34.2 HZ, which only appears in 0.1*C*-0.6*C*, is the result of extending and retracting of the leading-edge attached cavity. The violent development and the collapsing phenomenon of leading-edge cavitation lead to the peak value of PSD from D1 to D5 and fast dissipating of that behind D6. What is different at the peak value of 17.1 HZ is that it is the influence of trailing vortex shedding and collapsing and all monitor points below the hydrofoil remain a relatively high value of PSD at 17.1HZ. The specific peak values of PSD of 20 points for σ=0.65 is showing in Fig. 13. For 17.1HZ and 34.2HZ, acoustic PSD abruptly drops to extremely small values behind the hydrofoil tail. Besides, it can be observed that the peak value of PSD which up to 800000dB induced by shedding and collapsing of trailing vortex extending is comparatively higher than the peak value induced by retracting of leading-edge cavitation.

As shown in Fig. 14, only one peak value of PSD of 6.4HZ can be detected at σ=1.075 and this is consistent with the evolution of sheet cavitation. Additionally, as presented in Fig. 15, point D4 shows the highest peak value of PSD of 6.4HZ and the location of D4 is closely behind the cavitation growth and collapsing point.

4.3.2 Alleviations of the Noise by Ventilated Cavitation

Injected air flow rate of 250L/min, 375L/min and 500L/min are investigated to discuss the alleviation and acoustic pattern of ventilated cavitation.

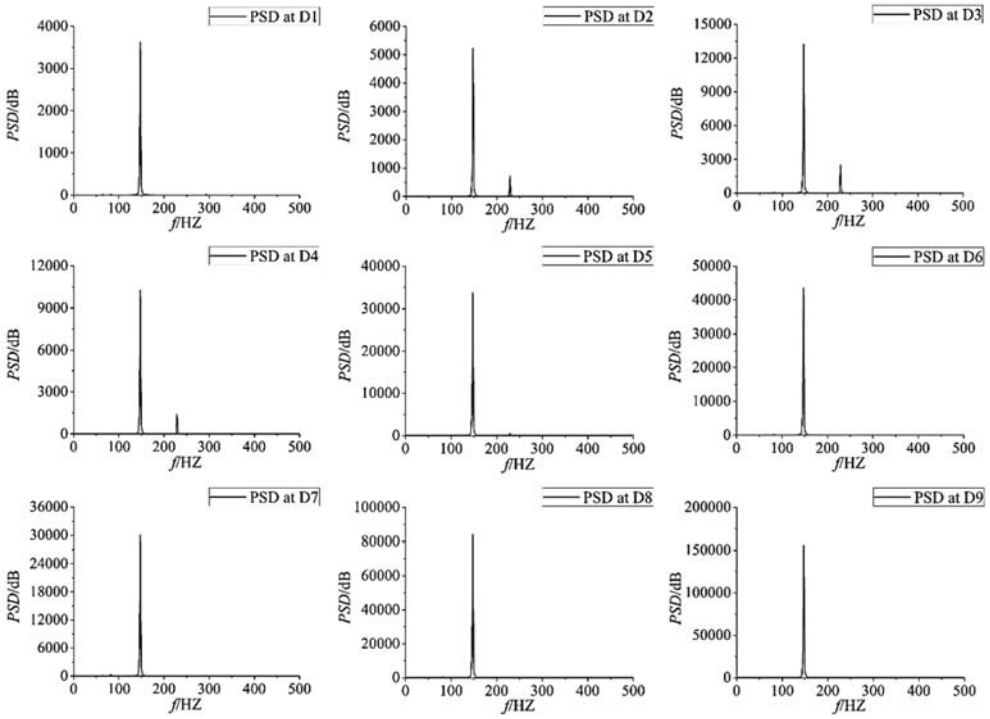

Fig. 16. PSD of 9 points for injected airflow rate of 250L/min.

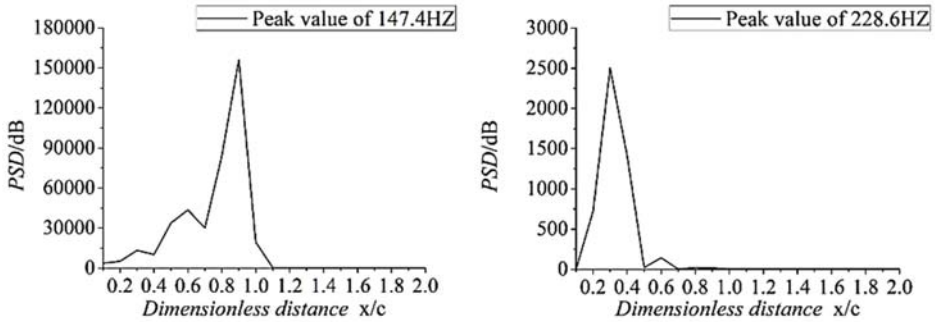

Fig. 17. Peak value of PSD of 20 points for injected airflow rate of 250L/min.

It can be seen from Figs. 16 and 17 that for air injection volumes of V_{air}=250L/min, two peak values of PSD are identified. The higher frequency peak which is induced by the leading edge attached cavity only appears on points D2 to D4. However, the lower frequency noise induced by periodic unsteady cloud near the hydrofoil trailing edge appears mainly on points near the tail of the hydrofoil. When comparing the specific peak values of PSD of 20 points in Fig. 17, it is obvious that the peak value of 117.4HZ is about one order higher than the peak value of 228.6HZ. This means lower frequency noise induced by periodic unsteady cloud near the trailing edge is larger than the noise induced by sheet cavity attaching to the leading edge and this is consistent with the phenomenon that the morphologic change of unsteady cloud near the trailing edge. Besides, PSD abruptly drops to extremely small values behind the hydrofoil tail and it is identical with the condition of nature cavitation.

While comparing Fig. 13 and Fig. 17, it is indicated that with the injected airflow rate of 250L/min, the PSD decreases from 800000dB to 150000dB. This means air injection is really an effective way to alleviate the noise, although the injected air induced new noises.

For injected airflow rate of V_{air}=375L/min, two peak values of PSD are identified, as showing in Fig. 18 and Fig. 19. The higher frequency peak which is induced by sheet cavity attaching to the leading edge mainly appears on points D4 and D5. Compared with the condition of V_{air}=250L/min, the occurrence location of the peak value of PSD moves backward in the direction of the flow. This phenomenon is corresponding to the morphologic change that the sheet cavity attaching to the leading edge gets longer and thicker. What' more, the peak

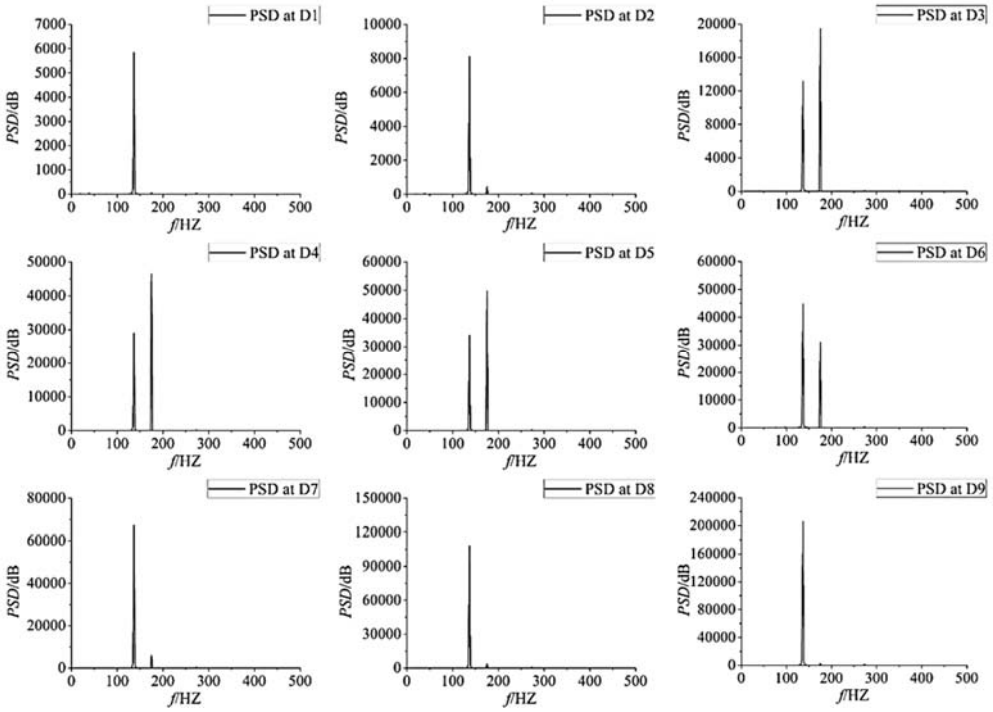

Fig. 18. PSD of 9 points for σ=0.65 and V_{air}=375L/min.

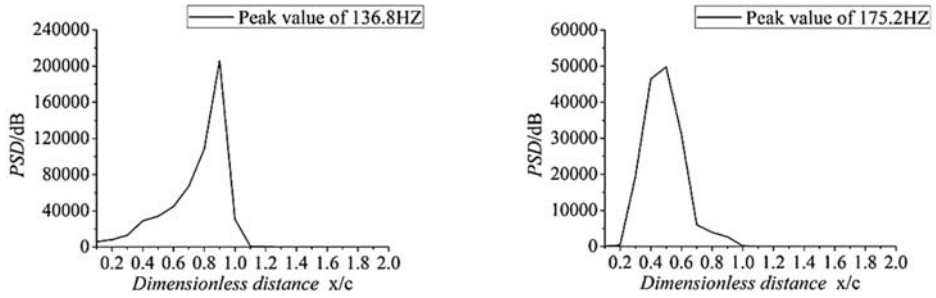

Fig. 19. Peak value of PSD of 20 points for V_{air}=375L/min.

value of PSD near the leading-edge increase from about 2500dB to 45000dB when injected airflow rate rises from 250L/min to375L/min. Lower frequency noise induced by periodic unsteady cloud near the trailing edge appears mainly on points D9 near the tail of hydrofoil which is the same as that of the former condition. Besides, the lower frequency noise gets stronger when air injection volume rises from 250L/min to375L/min.

For V_{air}=500L/min, only one peak value of PSD can be identified, as showing in Fig. 20 and Fig. 21. Additionally, peak values of PSD on monitor points D5 and D8 are much higher and that of other monitor points. It can be concluded that the noise of 145.3HZ is the result of the superposition of noise from the sheet cavity attaching to the leading edge and the noise-induced by an unsteady cloud near the trailing edge.

Compared with V_{air}=250L/min and 375 L/min, the noise-induced by sheet cavity attaching to the leading edge which is the higher frequency noise increase dramatically. It can be concluded that more air injected from the slot contribute to lager morphologic change of sheet cavity attaching to the leading edge and radiating larger noise.

The noise-induced by the unsteady cloud near the trailing edge also gets larger with the increasing of ventilation volume though the extent is not as much as the higher frequency noise. This is accordant with the simulation result that the unsteady cloud gets more violent near the trailing edge, though the morphology change of trailing vortex is not that evident.

5. CONCLUSION

The evolution of ventilated cavitation around a

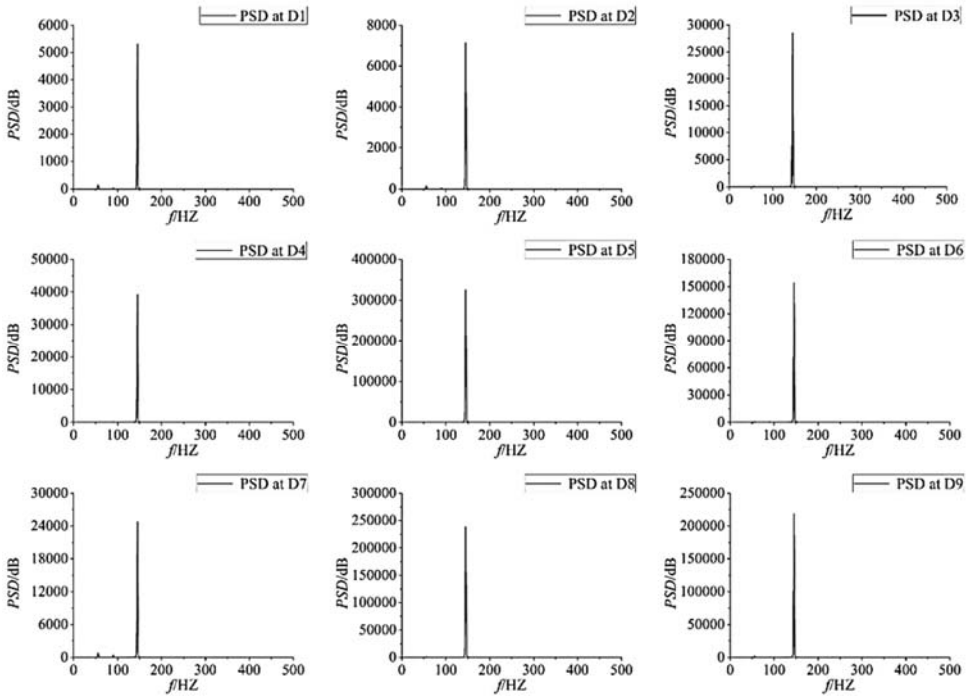

Fig. 20. PSD of 9 points for σ=0.65 and V_{air}=500L/min.

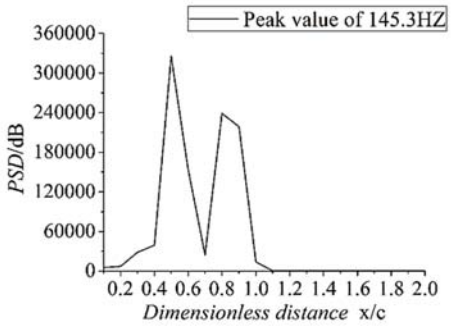

Fig. 21. Peak value of PSD of 20 points for V_{air}=500L/min.

NACA0015 hydrofoil and the flow-induced noise were investigated using the modified simulation method which considered the surface tension and non-condensable air. The experiment phenomena are well reproduced by the numerical simulation. The conclusions are as follows:

(1) With air injected into the flow, the sheet cavitation and cloud cavitation are disrupted and nature cavitation changes to ventilation cavitation. The ventilated cavitation consists of two parts: the attached cavity attached to the leading edge of the hydrofoil and the detached cavity which detached from the hydrofoil surface. With the increase of the injected air flow rate, the bubbles detached from the leading edge become larger. Compared with the natural cavitation, the re-entrant jet is too weak to cut off the attached cavity and its impact makes the attached cavity wavy. What's more, two opposite vortexes fall off in turn near the hydrofoil surface and make the ventilated cavity evolving periodically.

(2) Air injection can alleviate the pressure fluctuations induced by natural cavitation with suitable air flow rate, although the injected air induced new pressure fluctuations. The gaseous phase volumetric acceleration is proportional to the pressure fluctuations induced by ventilation cavitation. Among three ventilation volumes, injected airflow rate of 250L/min (σ=0.65) presents the best alleviation on pressure fluctuation induced by cloud cavitation and ventilation is not capable to suppress the pressure fluctuation of sheet cavitation (σ=1.075).

(3) Air injection can alleviate the flow noise induced by natural cavitation with suitable air

flow rate, although new noise can be excited by ventilation. With air injection, the frequency of noise radiated by leading edge sheet cavity is higher than that radiated by trailing edge unsteady cloud cavity for injected airflow rate of 250 L/min and 375 L/min. But the frequencies of these two kinds of noise overlap when V_{air}=500 L/min. With more air injected from the slot, the lower frequency noise induced by the leading edge sheet cavity and the higher frequency noise induced by trailing edge unsteady cloud cavity both increased.

ACKNOWLEDGMENTS

This research was funded by the National Natural Science Foundation of China (Project No. 51806058) and the Fundamental Research Funds for the Central Universities (Project No. B200202170).

REFERENCES

Bal, S., S. Kinnas and H. Lee (2001). Numerical analysis of 2-D and 3-D cavitating hydrofoils under a free surface. *Journal of Ship Research* 45, 34-49.

Blume, M. and R. Skoda (2019). 3D flow simulation of a circular leading edge hydrofoil and assessment of cavitation erosion by the statistical evaluation of void collapses and cavitation structures. *Wear* 428, 457-469.

Chen, X. and C. Lu (2005). Numerical simulation of ventilated cavitating flow around 2D foil. *Journal of Hydrodynamics* 17, 607-614.

Cheng, F., W. Ji, C. Qian and J. Xu (2018). Cavitation bubbles dynamics and cavitation erosion in water jet. *Results in Physics* 9, 1585-1593.

Dular, M., B. Stoffel and B. Sirok (2006). Development of a cavitation erosion model. *Wear* 261, 642-655.

Gao, Y., B. Huang, Q. Wu and G.Y. Wang (2015). Experimental investigation of the vibration characteristics of hydrofoil in cavitating flow. *Chinese Journal of Theoretical and Applied Mechanics* 47, 1009-1016.

Guo, J., C. Lu, Y. Chen and J. Cao (2010). Study of ventilated cavity morphology in different gas leakage regime. *Journal of Hydrodynamics* 22(5), 820-826.

Ji, B., X. W. Luo, R. Arndt and Y. L. Wu (2014). Numerical simulation of three dimensional cavitation shedding dynamics with special emphasis on cavitation-vortex interaction. *Ocean Engineering* 87, 64-77.

Ji, B., X. W. Luo, Y. L. Wu, X. X. Peng and H. Y. Xu (2010). Numerical and experimental study on unsteady shedding of partial cavitation. *Modern Physics Letter B* 41, 651-659.

Ji, N., H. Cheng, B. Huang, X. Luo, X. Peng and X. Long (2018). Research progresses and prospects of unsteady hydrodynamics characteristics for cavitation. *Advances in Mechanics* 49, 428-479.

Karn, A., C. Ellis, J. Hong and R. Arndt (2014). Investigations into the turbulent bubbly wake of a ventilated hydrofoil: Moving toward improved turbine aeration techniques. *Experimental Thermal Fluid Science* 64, 186-195.

Kato, H., A. Konno, M. Maeda and H. Yamaguchi (1996). Possibility of quantitative prediction of cavitation erosion without model test. *Journal Fluid Engineering-T. ASME* 118, 582-588.

Kawanami, Y., H. Kate, H. Yamaguchi, M. Yanimura and Y. Tagaya (1997). Mechanism and control of cloud cavitation. *Journal Fluid Engineering-T ASME* 119, 788-794.

Kim, S., C. Cheong and W. Park (2017). Numerical investigation on cavitation flow of hydrofoil and its flow noise with emphasis on turbulence models. *Aip Advances* 7, 14.

Kim, S., C. Cheong and W. Park (2018). Numerical Investigation into Effects of Viscous Flux Vectors on Hydrofoil Cavitation Flow and Its Radiated Flow Noise. *Applied Sciences-Basel* 8, 26.

Kim, S., C. Cheong, W. Park and H. Seol (2016). Numerical Investigation of Cavitation Flow around Hydrofoil and Its Flow Noise. *Transactions of the Korean Society for Noise and Vibration Engineering* 26, 141-147.

Kopriva, R., E. Arndt and E. L. Amromin (2008)Improvement of hydrofoil performance by partial ventilated cavitation in steady flow and periodic gusts. *Journal of Fluid Engineering-T. ASME* 130(3) 031301.Kravtsova, A., D. Markovich, K. Pervunin, M. Timoshevskiy and K. Hanjalic (2014). High-speed visualization and PIV measurements of cavitating flows around a semi-circular leading-edge flat plate and NACA0015 hydrofoil. *International Journal of Multiphase Flow* 60, 119-134.

Ku, G., C. Cheong, S. Kim, C. Ha and W. Park (2017a) Numerical Study on Cavitation Flow and Noise in the Flow Around a Clark-Y Hydrofoil. *Transactions of the KSME-A*, 41, 87-94.

Ku, G., R. Yoon and C. Cheong (2017b). Numerical investigation into cavitation flow noise of hydrofoil using quadrupole-corrected Ffowcs Williams and Hawkings equation. *Journal of Acoustical Society of Korea* 37, 263-270.

Lee, S., K. Kawakami and R. Arndt (2013). Measurements in the Wake of a Ventilated Hydrofoil. *Proceedings of the Asme Fluids Engineering Division Summer Meeting*.

Li, D. Y., R. Gong, H. Wang, J. Zhang, X. Wei and

L. Shu (2016). Numerical investigation in the vaned distributor under different guide vanes openings of a pump turbine in pump mode. *Journal of Applied Fluid Mechanics* 9(1), 253-266.

Li, Z., D. Ni and M. Yang (2015). Association Research on Characteristics of Cavitation Flow Structure and Pressure Pulsation around Hydrofoil. *Journal of Engineering Thermophysics* 36, 1005-1010.

Liu, M., L. Tan and S. L. Cao (2019). Cavitation-Vortex-Turbulence Interaction and One-Dimensional Model Prediction of Pressure for Hydrofoil ALE15 by Large Eddy Simulation. *Journal of Fluid Engineering-T.ASME*, 141, 17.

Liu, T., B. Huang, G. Wang and M. Zhang (2018) Experimental investigation of ventilated partial cavitating flows with special emphasis on flow pattern regime and unsteady shedding behavior around an axisymmetric body at different angles of attack. *Ocean Engineering* 147, 289-303.

Long, X. P., H. Y. Cheng, B. Ji and R. Arndt (2017). Numerical investigation of attached cavitation shedding dynamics around the Clark-Y hydrofoil with the FBDCM and an integral method. *Ocean Engineering* 137, 247-261.

Luo, X. W., B. Ji and Y. Tsujimoto (2016). A review of cavitation in hydraulic machinery. *Journal of Hydrodynamics* 28, 335-358.

Pendar, M. and E. Roohi (2016). Investigation of cavitation around 3D hemispherical head-form body and conical cavitators using different turbulence and cavitation models. Ocean Engineering 112, 287-306.

Qin, S. J., Y. Wu, D. Z. Wu and J. R. Hong (2019). Experimental investigation of ventilated partial cavitation. *International Journal of Multiphase Flow* 113, 153-164.

Seo, J., Y. Moon and B. Shin (2018). Prediction of cavitating flow noise by direct numerical simulation. *Journal of Computational Physics* 227, 6511-6531.

Wang, G., I. Senocak, W. Shyy, T. Ikohagi and S. Cao (2001). Dynamics of attached turbulent cavitating flows. *Progress in Aerospace Sciences* 37(6), 551-581.

Yu, A., X. C. Wang, Z. P. Zou, Q. H. Tang, H. X. Chen and D. Q. Zhou (2019). Investigation of Cavitation Noise in Cavitating Flows around an NACA0015 Hydrofoil. *Applied Sciences* 9, 3736.

Zhang, D., H. Wang, L. Geng and W. Shi (2015). Detached eddy simulation of unsteady cavitation and pressure fluctuation around 3-D NACA66 hydrofoil. *Thermal Science* 19, 1231-1234.

Zhou, H., M. Xiang, W. Zhang, X. Xu, K. Zhao and S. Zhao (2019). Interaction between Natural and Ventilated Cavitation around a Base Ventilated Hydrofoil. *Journal of Applied Fluid Mechanics*, 12(6), 1873-1883.